Universe Scientific Publishing

Single-Column Simulation of the Effect of Different Boundary Layer Turbulence Parameterization Schemes on Surface Sensible Heat Fluxes

Jinhua Zhong[1], Zhenhai Guo[2], Debin Su[1]

1. Chengdu University of Information Technology, Chengdu 610225, China.
2. Institute of Atmospheric Physics, Chinese Academy of Sciences, Beijing 100029, China.

Abstract: In this study, different turbulence parameterization schemes are simulated and compared using a single-column model to investigate their effects on the surface sensible heat flux. The Wangara Boundary Layer Experiment and The First International Satellite Land Surface Climatology Project Field Experiment (FIFE) were used. Eight different turbulence closure schemes were used for validation and comparison. These include six first-order closure schemes, one turbulent kinetic energy (TKE) closure scheme and the Reynolds stress second-order closure scheme. In this paper, the results of the second-order closure solved by the Reynolds stress equation are used as a benchmark. Since different turbulence closure schemes have different ability to capture turbulence, which in turn affects the turbulence transport ability and influences the heat transport process. The simulation results show that the difference in simulated temperature profiles between different turbulence parameterization schemes is not significant as the complexity of turbulence parameterization increases. However, this difference feeds back to the surface temperature, turbulent velocity scale and turbulent temperature scale, which affects the variation of the sensible heat flux. As the simulation integration time changes, the difference between the first-order closure scheme and the Reynolds stress scheme gradually increases due to the lack of turbulence portrayal. The results of the TKE scheme and the Reynolds stress scheme are more closely matched with the tendency of the root-mean-square error being smaller, and on the second day both schemes simulate the turbulence better.

Keywords: Turbulence Parameterization; Boundary Layer; Sensible Heat Flux; Single-Column Model

1. Introduction

The Planetary Boundary Layer (PBL) is the portion of the troposphere near the bottom of the subsurface troposphere, with a thickness of about a few hundred meters to 1-2 km, which is directly influenced by the Earth's surface on short time scales and exhibits pronounced turbulent properties (Garratt, 1994; Stull, 1988). Turbulent eddies within the boundary layer strongly influence momentum, heat, and water vapor transport between the surface and the atmosphere and control many important feedbacks between the subsurface and the atmosphere (Jia et al., 2023). Although the spatial and temporal scales of turbulent eddies are orders of magnitude smaller than climate-related scales, the sensible and latent heat fluxes induced by turbulent eddies are an important component of the global energy balance (Güttler et al., 2014). These interactions are often neglected for short-term projections in climate models such as general circulation models (GCM), but they are important in long-term projections and studies related to climate dynamics (Shin et al., 2018).

With the advancement of numerical simulation techniques, different turbulence parameterization schemes have been developed. The main difference being that the turbulence closure problem is solved differently, leading to differences in the vertical transport processes of momentum and heat and water vapor, which cause differences in the simulation results. The turbulence parameterizations used in large-scale atmospheric numerical models are mainly classified into first-order closure or first-and-a-half closure schemes (Shin & Hong, 2011). First-order closure is based on a semi-empirical approximation, and its limitation is that it is usually based on linear assumptions. However, real turbulence often involves nonlinear interactions, and first-order closure is difficult to capture these complex nonlinear relationships and is weak against large eddy transport in unstable boundary layers. Theoretically, the higher the order of the turbulence closure model, the more accurate the description of the turbulence process in the boundary layer, but the higher order closure also requires more expensive computational costs.

Many studies have confirmed that the results of large-scale weather models and climate prediction models are very sensitive to the

boundary layer turbulence parameterization used (Davy, 2018). Sánchez, Yagüe, and Gaertner (2007) analyzed the Regional Climate Model (RCM) model f first-and-a-half scheme compared to the GCM first-order closure scheme, and the TKE closure scheme in the RCM model has the advantage of turbulent kinetic energy as a predictor variable. Qiu (2013) conducted a simulation study of the alpine grassland region of the Tibetan Plateau and found that the net radiative flux, sensible and latent heat fluxes simulated by the MYNN2.5 scheme were optimal. Huang and Peng (2017) made the turbulent sensible heat flux calculation more detailed by improving the turbulence length formula in the MYNN scheme and considering the third-order turbulent flux term in the forecast variance of turbulent heat flux. The improved scheme reasonably solves the problem that the original scheme overestimates the turbulent momentum and heat of the boundary layer on the complex underlying surface in China. Therefore, a precise representation of turbulent transport is essential for reliable weather and climate models. This will improve the accuracy and predictive power of climate models.

This paper constructs a single-column model. The model includes six first-order closure schemes, one TKE closure scheme and a second-order Reynolds stress closure scheme, and the results of the second-order Reynolds stress scheme are used as the benchmark for comparison. In addition, the model also includes shortwave radiation scheme, longwave radiation scheme, surface layer parameterization scheme and land surface process scheme interacting with the atmosphere. The ability of different turbulence parameterization schemes to simulate sensible heat flux was evaluated using Wangara and FIFE sounding data. It provides a reference for further improving and perfecting the boundary layer turbulence parameterization scheme in the climate model.

2. Description of Model

2.1 One-dimensional atmospheric boundary layer governing equations

Assuming that the atmosphere is horizontally homogeneous, the set of equations controlling the boundary layer of the atmosphere can be written as:

$$\frac{\partial \bar{U}}{\partial t} = \frac{\partial}{\partial z}(-\overline{w'u'}) + f\bar{V} - fV_g \tag{1}$$

$$\frac{\partial \bar{V}}{\partial t} = \frac{\partial}{\partial z}(-\overline{w'v'}) - f\bar{U} + fU_g \tag{2}$$

$$\frac{\partial \overline{\Theta_v}}{\partial t} = \frac{\partial}{\partial z}(-\overline{w'\theta_v'}) + \frac{1}{\rho C_P}\frac{\partial R}{\partial z} \tag{3}$$

$$\frac{\partial \bar{Q}}{\partial t} = -\frac{\partial}{\partial z}(\overline{w'q'}) \tag{4}$$

Where the forecast variables U、V、Θ_v、Q are the east-west and north-south horizontal wind components, the virtual potential temperature, and the specific humidity, respectively. U_g and V_g are the components of the geostrophic winds, f is a Coriolis, ρ is the air density, C_p is the constant-pressure specific heat of dry air, and R is the net atmospheric longwave radiation. In case Wangara, $f = -0.826\times10^{-4}S^{-1}$, in case FIFE, $f = 0.914\times10^{-4}s^{-1}$. The downward longwave radiation is based on the RRTM (Rapid Radiative Transfer Model) longwave radiation scheme (Mlawer, Taubman, Brown, Iacono, & Clough, 1997). For the shortwave radiation scheme refer to Dudhia (1989).

The first term on the right-hand side of the equation is the turbulent flux term, with the upper line indicating the Reynolds mean. A general expression for the parametrized vertical turbulent flux can be written as:

$$\frac{\partial \bar{C}}{\partial t} = -\frac{\partial}{\partial z}\overline{w'c'} = \frac{\partial}{\partial z}\left[K_c\left(\frac{\partial \bar{C}}{\partial z}\right)\right] \tag{5}$$

Where C represents the mean value of the quantity (C; u, v, θ, q). where K_c and denote the turbulent transport coefficients of momentum and heat (K_M,K_H). In the present study, it has been assumed that K_M=K_H.

2.2 First-order closure parameterization schemes

This method is widely utilized as a common parametrization approach in atmospheric modelling. The scheme applies the K-theory

to express the second-order terms in the set of basic control equations for the atmospheric boundary layer in terms of the turbulence transport coefficients. The parameterization scheme for K_M is based on the classical mixing length theory scheme (Blackadar, 1962):

$$K_M = l^2 S = l^2 \left[\left(\frac{\partial \bar{u}}{\partial z} \right)^2 + \left(\frac{\partial \bar{v}}{\partial z} \right)^2 \right]^{1/2} \quad (6)$$

Where S denotes wind shear and l denotes the turbulent mixing length characterizing the energy containing eddies. Some of the first-order schemes refer to the parameterized schemes appearing in the articles by Holt and Raman (1988):

(1) Based on the scheme of Estoque and Bhumralkar (1970), hereafter referred to as EQ1970.

$$\begin{cases} K_M = l^2 S(1 - 3Rib) & Rib < 0 \\ K_M = l^2 S(1 + 3Rib)^{-1} & Rib \geq 0 \end{cases} \quad (7)$$

Here Rib denotes the gradient Richardson number and is defined as:

$$\text{Rib} = \frac{g z_1}{\theta} \frac{(\theta_1 - \theta_s)}{|U_1|^2} \quad (8)$$

Here z_1、θ_1、U_1 denotes the values at the bottom height of the model, θ_s denotes the surface temperature, and g is the acceleration.

(2) Based on the scheme of Holt and Raman (1988), hereafter referred to as Dj1974.

$$\begin{cases} K_M = l^2 S(1 - Rib)^{\frac{1}{2}} & Rib < 1 \\ K_M = 0 & Rib \geq 1 \end{cases} \quad (9)$$

(3) Based on the scheme of Louis (1979), hereafter referred to as Louis1979.

$$\begin{cases} K_M = l^2 S\left(1 - \frac{10Rib}{1 + 5\sqrt{Rib}}\right) & Rib < 0 \\ K_M = l^2 S\left(\frac{1}{1 + 5Rib}\right)^2 & Rib \geq 0 \end{cases} \quad (10)$$

(4) Based on the scheme of Bhumralkar (1975), hereafter referred to as BH1975.

$$\begin{cases} K_M = l^2 S(1 - 18Rib) & \frac{\partial \theta}{\partial z} < 0 \\ K_M = l^2 S(1 + 18Rib)^{-1} & \frac{\partial \theta}{\partial z} \geq 0 \end{cases} \quad (11)$$

(5) Based on the scheme of Holtslag and Boville (1993), hereafter referred to HS1993.

$$\begin{cases} K_M = l^2 S\left(\frac{1}{1 + 10Rib(1 + 8Rib)}\right) & Rib < 0 \\ K_M = l^2 S\sqrt{1 - 18Rib} & Rib \geq 0 \end{cases} \quad (12)$$

(6) Based on the scheme of Zhang and Anthes (1982), hereafter referred to BLK1979.

$$\begin{cases} K_M = \frac{1.1 l^2 S(Ric - Rib)}{Rib} & Rib < Ric \\ K_M = K_0 & Rib < Ric \end{cases} \quad (13)$$

Here K_0 is taken to be the smaller background value of 0.0093, Ric is the key Richardson number, taken to be 0.25.

2.3 TKE closure parameterization schemes

Another commonly used closure scheme in K-theory is the TKE closure scheme. It considers K_m proportional to the square root of the turbulent kinetic energy:

$$K_m = c_0 l E^{\frac{1}{2}} \quad (14)$$

Where is a constant, E is the turbulent kinetic energy, and remains the mixing length, which can be either forecast or diagnostic. The parameterization of here refers to Therry and Lacarrère (1983). Differences in and in different schemes affect the simulation results:

$$\frac{\partial E}{\partial t} = -\frac{1}{\rho} \frac{\partial}{\partial z} \overline{w'e'} - \overline{u'w'} \frac{\partial u}{\partial z} - \overline{v'w'} \frac{\partial v}{\partial z} + \beta \overline{w'\theta'} - \varepsilon \quad (15)$$

Where E is the turbulent kinetic energy, u',v',w' are the horizontal and vertical pulsation velocities. θ' is the temperature pulsation velocities, β is the buoyancy coefficient, and ε is the rate of dissipation of the turbulent kinetic energy. the first term on the right-hand side of the equation denotes the TKE of the turbulence transport, the second and third terms are the TKE produced by the wind shear, the fourth term is the TKE of buoyancy depletion, and the last term is the TKE consumed by molecular diffusion.

2.4 Second-order closure parameterization schemes

The second-order turbulence closure model is a prediction equation that adds all the relevant second-order correlation terms on the basis of the predicted average, and the higher-order terms appearing in the second-order prediction equation are expressed by the corresponding second-order correlation terms. The second-order closed parametric framework used in this paper is:

(1) Reynolds stress term($\overline{u'u'}$、$\overline{v'v'}$、$\overline{w'w'}$、$\overline{u'v'}$、$\overline{u'w'}$、$\overline{v'w'}$):

$$\frac{D\left(\overline{u_i'u_j'}\right)}{Dt} = -\left(\overline{u_i'u_k'}\frac{\partial \bar{u}_j}{\partial x_k} + \overline{u_j'u_k'}\frac{\partial \bar{u}_i}{\partial x_k}\right) - \left(\frac{g_i}{\bar{\theta}}\overline{\theta_v'u_j'} + \frac{g_j}{\bar{\theta}}\overline{\theta}_i\right) - \frac{\partial}{\partial x_k}\left[\overline{u_i'u_j'u_k'} + \frac{1}{\rho_0}p\left(\delta_{jk}'u_i' + \delta_{ik}'u_k'\right)\right] - 2\gamma\frac{\partial \bar{u}_i}{\partial x_k}\frac{\partial \bar{u}_j}{\partial x_k} + \frac{1}{\rho_0}P\left(\frac{\partial \bar{u}_i}{\partial x_j} + \frac{\partial \bar{u}_j}{\partial x_i}\right) \quad (16)$$

(2) Turbulent heat flux term equation ($\overline{u'\theta'}$、$\overline{v'\theta'}$、$\overline{w'\theta'}$):

$$\frac{D\overline{u_i'\theta'}}{Dt} = -\left(\overline{u_i'u_k'}\frac{\partial \bar{\theta}}{\partial x_k}\right) - \overline{\theta'u_k'}\frac{\partial \bar{u}_i}{\partial x_k} - \frac{g_i}{\bar{\theta}}\overline{\theta'\theta_v'} - \frac{\partial}{\partial x_k}\left(\overline{u_i'u_j'\theta'} - \delta_{ik}\frac{\overline{p\theta}}{\rho_0}\right) - \frac{1}{\rho_0}p\frac{\partial \bar{\theta}}{\partial x_i} \quad (17)$$

(3) Turbulent humidity flux term equation ($\overline{u'q'}$、$\overline{v'q}$、$\overline{w'q'}$):

$$\frac{D\overline{u_i'q'}}{Dt} = -\left(\overline{u_i'u_k'}\frac{\partial \bar{q}}{\partial x_k}\right) - \overline{q'u_k'}\frac{\partial \bar{u}_i}{\partial x_k} - \frac{g_i}{\bar{\theta}}\overline{q'\theta_v'} - \frac{\partial}{\partial x_k}\left(\overline{u_i'u_j'q'} - \delta_{ik}\frac{\overline{pq}}{\rho_0}\right) - \frac{1}{\rho_0}p\frac{\partial \bar{q}}{\partial x_i} \quad (18)$$

(4) Potential temperature and specific humidity interaction equation ($\overline{\theta'q'}$、$\overline{q'q'}$、$\overline{\theta'\theta'}$):

$$\frac{D\overline{ac}}{Dt} = -\left(\overline{au_k'}\frac{\partial \bar{c}}{\partial x_k}\right) - \overline{cu_k'}\frac{\partial \bar{a}}{\partial x_k} + \frac{\partial u_k'ac}{\partial x_k} - 2\varepsilon_{ab} \quad (19)$$

The letters to the left of the equal sign in the above equation represent the relevant meteorological element perturbations, the subscripts i, j = 1, 2, 3 correspond to the u, v, and w components, and γ is the dynamical viscosity coefficient. The first term on the right side of the equal sign is the shear generation term, the second indicates the buoyancy generation term, the third is the turbulent diffusivity term, the fourth is the turbulent dissipation term, and the fifth is the pressure-deformation term. The turbulence diffusivity, turbulence dissipation term and pressure-deformation term are new variables and need to be parameterized, for the detailed parameterization procedure refer to(Guo, Chen, Zhang, Chen, & Zhang, 1999).

2.5 The surface layer

The surface layer similarity theory is used to calculate the friction velocity u_*、turbulent temperature scale θ_*, and to estimate the momentum flux τ, sensible heat flux H ,

$$\tau = \rho u_*^2 = [(\overline{u'w'})^2 + (\overline{v'w'})^2]^{1/4} \quad (20)$$

$$\mathrm{H} = \rho c_p u_* \theta_* = \rho c_p \overline{\theta_v' w'} \quad (21)$$

The parameterization scheme for u_*、θ_* and q_* is as follow,

$$u_* = \frac{kU_1}{\ln\left(\frac{z_1}{z_0}\right) - \psi_M\left(\frac{z_1}{L}\right) + \psi_M\left(\frac{z_0}{L}\right)} \quad (22)$$

$$\theta_* = \frac{k(\theta_1 - \theta_s)}{\ln\left(\frac{z_1}{z_0}\right) - \psi_H\left(\frac{z_1}{L}\right) + \psi_H\left(\frac{z_0}{L}\right)} \quad (23)$$

z_0 is the surface roughness length and assumes that the roughness lengths of momentum and heat are the same, k is Kamen's constant taken as 0.4. $\psi_{M,H}$ is the dimensionless stability function of momentum and heat; and L is the Monin-Obukhov length. Refer to Paulson (1970) and Dyer (1974) for flux profile relations for the unsteady case (z/L<0) and Beljaars and Holtslag (1991) for the stable case (z/L>0). In case Wangara, z_0 = 0.01 cm, in case FIFE, z_0 = 0.065 cm.

Surface temperatures are required for the calculation of sensible heat fluxes and are used here to predict soil temperatures by solving the surface energy balance equation,

$$R_n + Q_E + H - G = 0 \quad (24)$$

Here R_n is the net radiative flux at the surface and G is the soil heat flux. Below the soil surface, the soil heat transfer equation is used to represent the vertical diffusion process in the soil. The surface specific humidity is solved using the surface water balance equation (Kim &

Ek, 1995).

3. Initial and boundary conditions

In this paper, two cases are selected for simulation research. The first simulation case is the radiosonde data of Wangara case from 06:00 LT on August 16 to 18:00 LT on August 17, which located in the arid region of eastern Australia (34°30′S, 144°56′E), with very sparse vegetation, and the weather on the day of the selected data is clear and the horizontal advection is very weak, which is a good test of the boundary layer and heat fluxes. The geostrophic winds refer to the interpolation equations given by Yamada and Mellor (1975). The second experiment was selected from the FIFE, which was conducted in 1987 and 1989 in eastern Kansas, USA (39.05°N, 96.53°W). Detailed information on the experiment can be found in Pleim and Xiu (1995). The initial profile for the individual FIFE cases was chosen to be 07:00 a.m. LT on 11 July 1987. The geostrophic winds were chosen to be those corresponding to an altitude of 2,000 m.

The lower boundary condition of the model's basic set of control equations is set to:

$$-K_M \frac{\partial \bar{u}}{\partial z}|z=0 = \overline{u'w'} = \cos\mu\, u_*^2 \quad (25)$$

$$-K_M \frac{\partial \bar{v}}{\partial z}|z=0 = \overline{v'w'} = \sin\mu\, u_*^2 \quad (26)$$

$$-K_H \frac{\partial \overline{\theta_v}}{\partial z}|z=0 = \overline{\theta_v' w'} = u_* \theta_* \quad (27)$$

$$-K_H \frac{\partial \bar{q}}{\partial z}|z=0 = \overline{q'w'} = u_*\, q_* \quad (28)$$

Here μ is the shear stress due to the horizontal wind, $\mu = \tan^{-1}\left(\frac{v}{u}\right)$. The fluxes under the corresponding third-order moments in the second-order closure are assumed to be zero, and the fluxes at the upper boundary are all set to zero. The initial values of soil temperature and moisture in the deepest part of the soil are fixed, and the boundary fluxes in the deepest part of the soil are set to zero.

The time step of the model is set to 10 s and the number of grids is 81, where the 41st layer to the simulated boundary layer is at a height of 2 km, and the bottom grid is set to 10 m. The system of equations is solved using a finite element computational method, using Crank-Nicolson as the numerical discretization method.

4. Model results

4.1 Turbulent diffusion coefficient and temperature profile

The turbulence parameterization process is mainly about determining the turbulent diffusion coefficient (TDC), which determines the local turbulent mixing strength and efficiency. While the evolution of momentum and heat and water vapor fluxes within the boundary layer is particularly affected by the TDC, which may lead to differences in the simulated boundary layer or even the whole model region(Jia et al., 2023). For the first-order closed model used in this paper causes the difference in TDC mainly from the effect of the stability function. Fig. 1(a ~ d) show the simulated TDC values at different times for the Wangara case. The first-order scheme shows slightly larger TDC at 09:00 a.m. on day 33(Fig. 1 a). With increased TDC for all schemes at noon due to stronger solar radiation. Different schemes exhibit varying TDC, indicating mixing efficiency. For instance, the DJ1974, Louis1979, and HS1993 schemes show relatively smaller TDC, suggesting less effective mixing (Fig. 1 b). At night, wind shear becomes prominent, affecting the first-order scheme more and resulting in larger TDC at 2300 h, while the second-order Reynolds stress scheme produces the weakest TDC (Fig. 1 d).

The magnitude of the turbulent mixing intensity to the boundary layer is most directly reflected in the vertical profile, as shown in Fig. 1(e ~ h). At 09:00, all first-order closure schemes underestimate lower layer temperature, but TKE and second-order closure schemes align better with observations. By 12:00, a convective boundary layer forms in modeled and measured profiles. BLK1979, BH1975, and ES1970 schemes exhibit similar temperature profiles to TKE and second-order closure, depicting more realistic turbulent mixing. DJ1974, Louis1979, and HS1993 schemes show insufficient mixing efficiency, with a shallower mixing layer. Although the TKE scheme overestimates mixing height, simulated profiles generally match observations, with Reynolds stress scheme closest to reality. Whereas the FIFE case produces similar results, the focus here is only on the Wangara case temperature profile.

4.2 The analysis of sensible heat flux, surface temperature, friction velocity and turbulent temperature scale

Fig. 2(a), shows the results of the simulation of sensible heat fluxes for the Wangara case, and b, shows the results of the simulation of surface temperatures for the Wangara case. The BH1975 and BLK1979 produce the largest sensible heat fluxes during the day in the first-order closure schemes, and the DJ1973 simulates the smallest sensible heat flux in the first-order closure scenario and the smallest among all schemes the next day. A large sensible heat flux means more heat transfer to the atmosphere, so the BLK1979, BH1975, TKE, and Reynolds stress schemes all show lower surface temperatures. While DJ1973, HS1993 show high surface temperature during the daytime, this may be because the lower TDC cannot efficiently transfer the heat from the surface to the boundary layer, and stagnates on the soil surface resulting in high soil temperature. In the FIFE case, similar results were produced as in the Wangara case. However, the difference between soil temperatures was more pronounced under wet conditions.

From Eq. (21), the parameterization of the sensible heat flux is related to u_* and θ_*. u_* is a physical quantity characterizing the strength of mechanical turbulence, and, θ_* characterizes the strength of buoyant turbulence. u_* is strongly affected by the wind speed, surface roughness, and stability, and θ_* is affected by the difference in geothermal air temperatures, the thermal roughness of the surface, and stability. For the simulation results in Fig. 2 (c) and (d) can be seen that the Reynolds stress scheme shows a larger u_* during the daytime, with the rest of the schemes being more consistent. At night it again shows the lowest u_*. This suggests that the remaining scenarios underestimate the generation of mechanical turbulence during the day. The Reynolds stress scheme produces the smallest θ_* during the day, followed by the TKE scheme. It shows that the other schemes overestimate the buoyancy forcing. The TKE scheme is closer to the Reynolds stress scheme in the simulation of buoyant turbulence. For Fig. 2(g、h) FIFE individual cases, the turbulence amount again appears different. The Reynolds stress scheme in Fig. 2(g) does not differ more significantly from the other schemes during the day, the differences are mainly at night. The Reynolds stress scheme at night is more consistent with the TKE scheme, exhibiting a smaller u_*. The simulation results of the individual schemes in Fig. 2(h) are more consistent for θ_* during the daytime, and the bump in the figure on the second day of the simulation is due to computational instability.

Table 1 shows the calculation of the root mean square error RMSE between the second-order Reynolds stress scheme and the other turbulence parameterization schemes, which is expressed as:

$$RMSE = \sqrt{\frac{1}{N}\sum_{i=1}^{n}\left(Y_i - f(x_i)\right)^2} \tag{29}$$

Where Y_i denotes the predicted value, $f(x_i)$ is the true value corresponding second order Reynolds stress scheme and N denotes the number of samples. The RMSE resulting from integrating for 1 hour, 12 hours, 24 hours and 36 hours were calculated respectively. From Table 1, the TKE scheme has the smallest RMSE for the first 1 hour of integration in Wangara case, and DJ1973 scheme exhibits the lowest RMSE for the first 12 and 24 hours of integration. However, the difference between the DJ1973 scheme starts to become larger in the 36 hours simulation, and the difference of the TKE scheme gradually decreases. TKE scheme differences gradually decrease. In the FIFE individual case, the TKE scheme has the lowest RMSE at all time points. In terms of the time variation of integration, the RMSE errors between most of the schemes and the second-order scheme are getting larger. The TKE scheme shows the smallest RMSE in the last 12 hours (24h-36h) of integration. RMSE. This also reflects the fact that the TKE scheme fits closer to the second-order scheme with time, and describes the turbulence more accurately than first-order closure schemes.

Table 1 Root-mean-square errors of sensible heat fluxes for seven turbulence parameterization schemes and Reynolds stress scheme.

RMSE	Wangara				FIFE			
	1h	12h	24h	36h	1h	12h	24h	36h
BLK1979	0.13	11.03	8.08	9.95	7.11	6.42	6.29	6.50
HS1993	1.66	4.48	3.98	4.24	4.96	5.27	6.79	6.58
BH1975	3.23	12.28	9.95	12.50	6.12	7.03	8.8	8.68
ES1970	6.47	11.98	11.45	12.86	16.38	6.31	11.49	10.40
Louis1979	2.67	7.34	6.21	6.53	7.09	5.15	7.85	7.32
DJ1973	0.22	2.54	2.76	4.26	18.87	10.54	9.08	8.70
TKE Closure	0.07	3.16	3.76	3.80	5.08	4.78	4.44	3.88

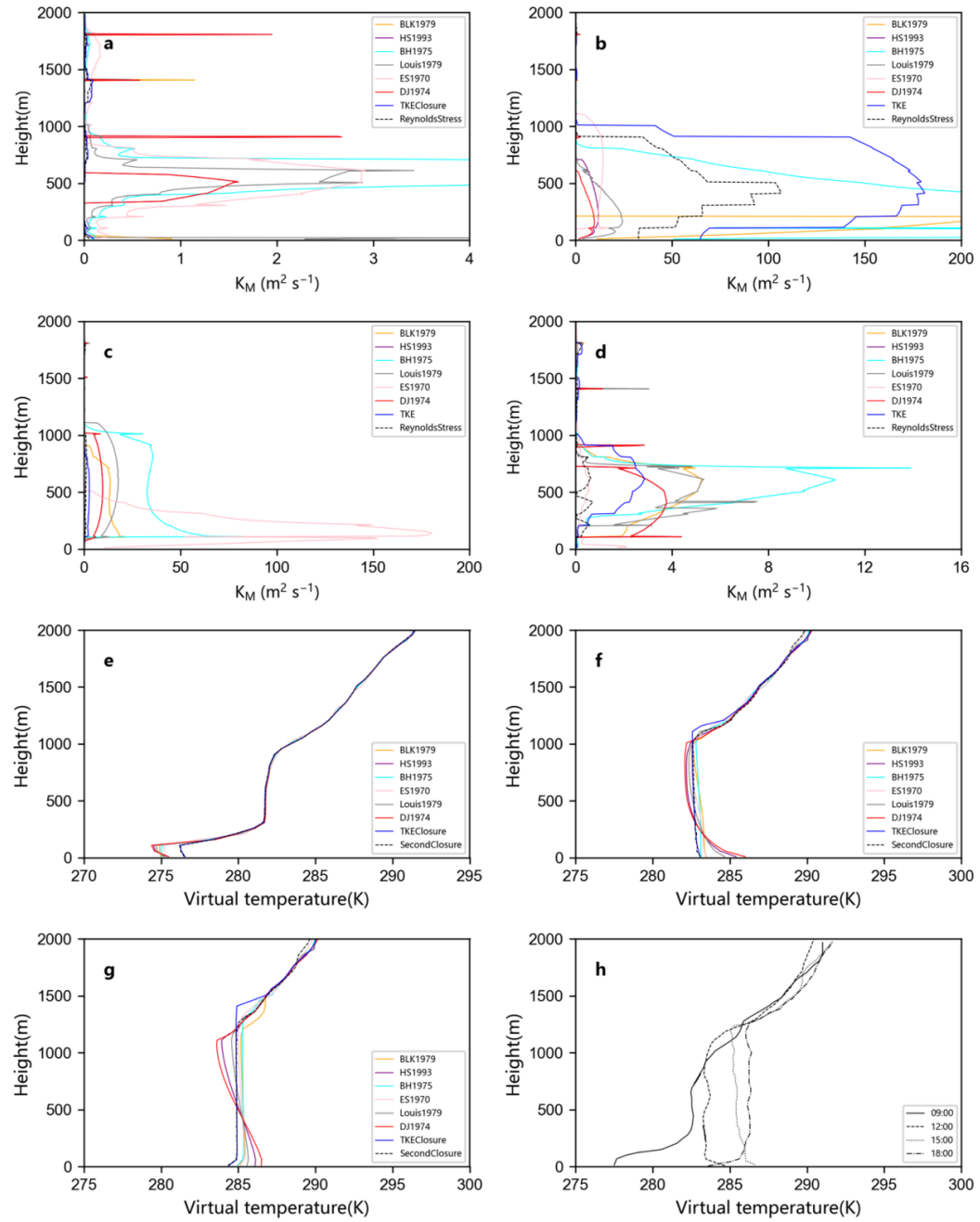

Fig. 1 Turbulent diffusion coefficients() for individual Wangara case (a) 0900 LT, (b) 1200 LT, (c) 1800 LT, (b) 2300 LT; Temperature profiles for individual cases of Wangara; (e) 0900LT, (f) 1200LT, (g) 1800LT, (h) Observations.

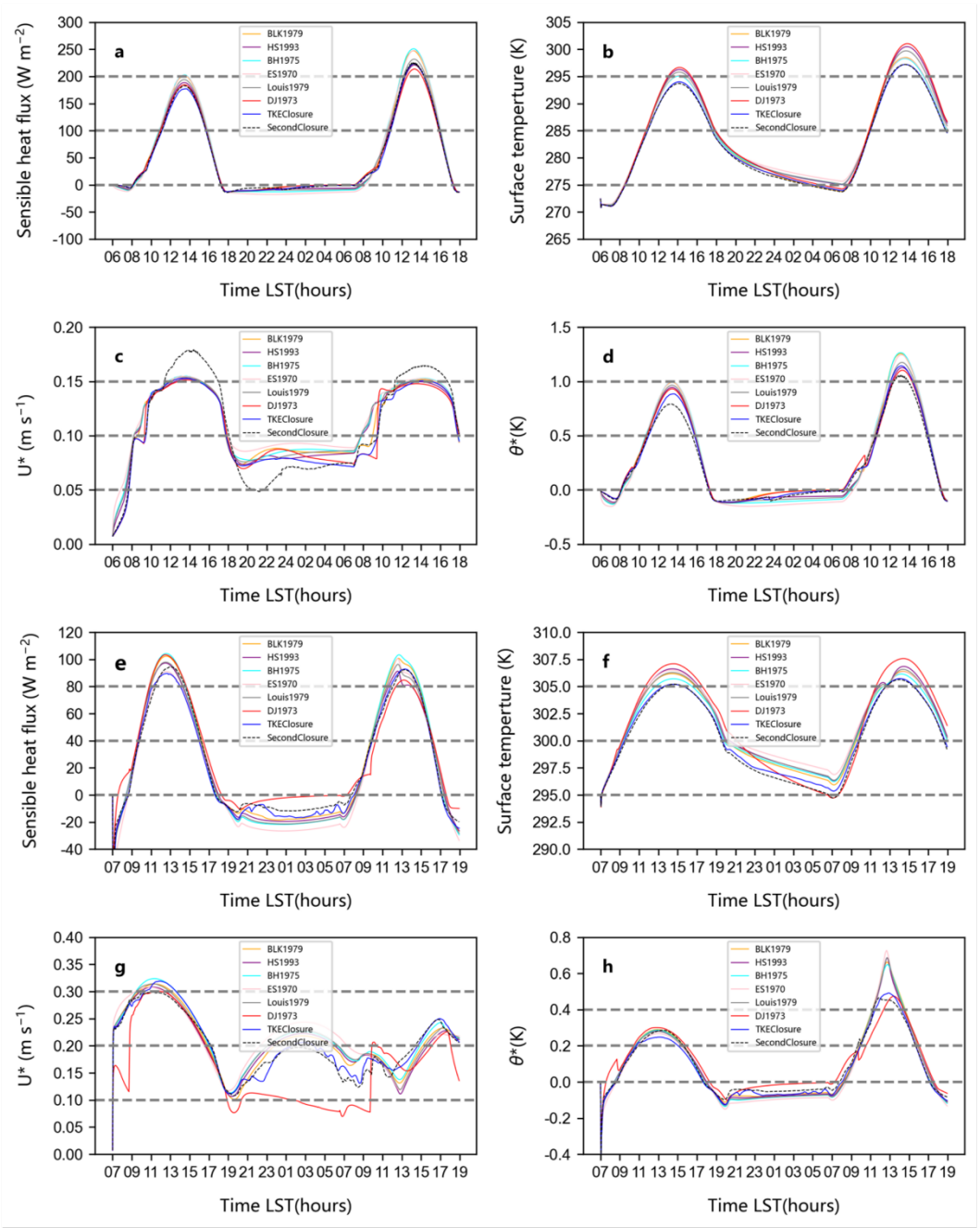

Fig. 2 Wangara case (a) Sensed heat flux, (b) surface temperature, (c) friction velocity, (d) turbulent temperature scale. FIFE case (e) sensible heat flux, (f) surface temperature, (g) friction velocity, (h) temperature scale.

5. Discussion and Conclusions

This paper focuses on the effects of different turbulent closure schemes interacting with the land surface model on the surface sensible heat flux. Different turbulence closure schemes make the TDC change greatly, which affects the ability of turbulent transport and leads to the change of momentum and thermodynamic variables.

When the turbulent diffusion mixing is good, there is no obvious gap between the first-order closure scheme and the high-order closure scheme on the average vertical profile, but the sensible heat flux can see a more obvious gap at noon during the day. This gap is mainly in the ability to simulate the turbulent quantities and . Therefore, the first-order closure scheme under the influence of mixing length, wind shear

and stability function alone cannot accurately represent the change of turbulence in PBL. With the change of integration time, the difference between the results of the sensible heat flux of the first-order closure simulation and the high-order closure scheme gradually increases. The higher-order closure model describes the complex nonlinear interactions of turbulent transport, which is better for turbulence simulation and better reflects the intrinsic laws of the turbulent transport process. The simulation results also show that the TKE can fit well with the Reynolds stress scheme, describe the surface-air interaction and the transport of each flux in the boundary layer better, make the surface -air energy exchange more realistic, and enable the atmosphere to obtain more effective heat flux at the surface.

Changes in the sensible heat flux caused by turbulence in turn play an important role in the global energy balance. With the improvement of computational power, there is a need for more in-depth research and refinement of boundary layer parameterization schemes, and the introduction of turbulence closure schemes with more accurate turbulence portrayal in global or regional models. This is of great significance for the accurate representation of boundary layer processes in large-scale models, and is conducive to improving the accuracy of numerical weather prediction as well as long-term climate simulation results.

References

[1] Beljaars, A. C. M., & Holtslag, A. A. M. (1991). Flux Parameterization over Land Surfaces for Atmospheric Models. Journal of Applied Meteorology and Climatology, 30(3), 327-341. doi:10.1175/1520-0450(1991)030<0327:FPOLSF>2.0.CO;2.

[2] Bhumralkar, C. M. (1975). Parameterization of the planetary boundary layer in atmospheric general circulation models. Reviews of Geophysics, 14(2), 215-226. doi:10.1029/RG014i002p00215.

[2] Davy, R. (2018). The Climatology of the Atmospheric Boundary Layer in Contemporary Global Climate Models. Journal of Climate, 31(22), 9151-9173. doi:10.1175/JCLI-D-17-0498.1.

[3] Dudhia, J. (1989). Numerical Study of Convection Observed during the Winter Monsoon Experiment Using a Mesoscale Two-Dimensional Model. Journal of The Atmospheric Sciences - J ATMOS SCI, 46, 3077-3107. doi:10.1175/1520-0469(1989)046<3077:NSOCOD>2.0.CO;2.

[4] Dyer, A. J. (1974). A review of flux-profile relationships. Boundary-Layer Meteorology, 7(3), 363-372. doi:10.1007/BF00240838.

[5] Estoque, M. A., & Bhumralkar, C. M. (1970). A method for solving the planetary boundary-layer equations. Boundary-Layer Meteorology, 1(2), 169-194. doi:10.1007/BF00185738.

[6] Garratt, J. R. (1994). Review: the atmospheric boundary layer. Earth-Science Reviews, 37(1), 89-134. doi:10.1016/0012-8252(94)90026-4.

[7] Guo, Z., Chen, C., Zhang, H., Chen, J., & Zhang, A. (1999). A One-Dimensional Finite Element Model with Two-Order Closure Scheme Simulating the Atmospheric Boundary Layer. Part I: Convective Boundary Layer. Chinese Journal of Atmospheric Sciences, 23(6), 733-744. doi:10.3878/j.issn.1006-9895.1999.06.10.

[8] Güttler, I., Branković, Č., O'Brien, T. A., Coppola, E., Grisogono, B., & Giorgi, F. (2014). Sensitivity of the regional climate model RegCM4.2 to planetary boundary layer parameterisation. Climate Dynamics, 43(7), 1753-1772. doi:10.1007/s00382-013-2003-6.

[9] Holt, T., & Raman, S. (1988). A review and comparative evaluation of multilevel boundary layer parameterizations for first-order and turbulent kinetic energy closure schemes. Reviews of Geophysics, 26(4), 761-780. doi:10.1029/RG026i004p00761.

[10] Holtslag, A. A. M., & Boville, B. A. (1993). Local Versus Nonlocal Boundary-Layer Diffusion in a Global Climate Model. Journal of Climate, 6(10), 1825-1842. doi:10.1175/1520-0442(1993)006<1825:LVNBLD>2.0.CO;2.

[11] Jia, W., Zhang, X., Wang, H., Wang, Y., Wang, D., Zhong, J., . . . Lin, Y. (2023). Comprehensive evaluation of typical planetary boundary layer (PBL) parameterization schemes in China – Part 2: Influence of uncertainty factors. Geosci. Model Dev., 16(22), 6833-6856. doi:10.5194/gmd-16-6833-2023.

[12] Kim, J., & Ek, M. (1995). A simulation of the surface energy budget and soil water content over the Hydrologic Atmospheric Pilot Experiments-Modélisation du Bilan Hydrique forest site. Journal of Geophysical Research: Atmospheres, 100(D10), 20845-20854. doi:10.1029/95JD01469.

[13] Louis, J.-F. (1979). A parametric model of vertical eddy fluxes in the atmosphere. Boundary-Layer Meteorology, 17(2), 187-202. doi:10.1007/BF00117978.

[14] Mlawer, E. J., Taubman, S. J., Brown, P. D., Iacono, M. J., & Clough, S. A. (1997). Radiative transfer for inhomogeneous atmospheres: RRTM, a validated correlated-k model for the longwave. Journal of Geophysical Research: Atmospheres, 102(D14), 16663-16682. doi:10.1029/97JD00237.

[15] Paulson, C. A. (1970). The Mathematical Representation of Wind Speed and Temperature Profiles in the Unstable Atmospheric Surface Layer. Journal of Applied Meteorology and Climatology, 9(6), 857-861. doi:10.1175/1520-0450(1970)009<0857:TMROWS>2.0.CO;2.

[16] Pleim, J. E., & Xiu, A. (1995). Development and Testing of a Surface Flux and Planetary Boundary Layer Model for Application in Mesoscale Models. Journal of Applied Meteorology and Climatology, 34(1), 16-32. doi:10.1175/1520-0450-34.1.16.

[17] Qiu. (2013). Applicability Research of Planetary Boundary Layer Parameterization Scheme in WRF Model over the Alpine Grassland Area. Plateau Meteorology, 32(1), 46-55. doi:10.7522/j.issn.1000-0534.2012.00006.

[18] Sánchez, E., Yagüe, C., & Gaertner, M. A. (2007). Planetary boundary layer energetics simulated from a regional climate model over Europe for present climate and climate change conditions. Geophysical Research Letters, 34(1). doi:10.1029/2006GL028340.

[19] Shin, H. H., & Hong, S.-Y. (2011). Intercomparison of Planetary Boundary-Layer Parametrizations in the WRF Model for a Single Day from CASES-99. Boundary-Layer Meteorology, 139(2), 261-281. doi:10.1007/s10546-010-9583-z.

[20] Shin, H. H., Ming, Y., Zhao, M., Golaz, J.-C., Xiang, B., & Guo, H. (2018). Evaluation of Planetary Boundary Layer Simulation in GFDL Atmospheric General Circulation Models. Journal of Climate, 31(13), 5071-5087. doi:10.1175/JCLI-D-17-0543.1.

[21] Stull, R. B. (1988). An Introduction to Boundary Layer Meteorology: Springer Dordrecht.

[22] Therry, G., & Lacarrère, P. (1983). Improving the Eddy Kinetic Energy model for planetary boundary layer description. Boundary-Layer Meteorology, 25(1), 63-88. doi:10.1007/BF00122098.

[23] Yamada, T., & Mellor, G. (1975). A Simulation of the Wangara Atmospheric Boundary Layer Data. Journal of Atmospheric Sciences, 32(12), 2309-2329. doi:10.1175/1520-0469(1975)032<2309:ASOTWA>2.0.CO;2.

[24] Zhang, D., & Anthes, R. A. (1982). A High-Resolution Model of the Planetary Boundary Layer—Sensitivity Tests and Comparisons with SESAME-79 Data. Journal of Applied Meteorology (1962-1982), 21(11), 1594-1609. doi:10.1175/1520-0450(1982)021<1594:AHRMOT>2.0.CO;2.